

# Readout of GEM Detectors Using the Medipix2 CMOS Pixel Chip

A. Bamberger<sup>a</sup>, K. Desch<sup>a,1</sup>, U. Renz<sup>a</sup>, M. Titov<sup>a,b</sup>,  
N. Vlasov<sup>a</sup>, P. Wienemann<sup>a,1</sup>, A. Zwerger<sup>a</sup>

<sup>a</sup>*Albert-Ludwigs University of Freiburg, Physics Institute, Freiburg, Germany*

<sup>b</sup>*Institute of Theoretical and Experimental Physics (ITEP), Moscow, Russia*

---

## Abstract

We have operated a Medipix2 CMOS readout chip, with amplifying, shaping and charge discriminating front-end electronics integrated on the pixel-level, as a highly segmented direct charge collecting anode in a three-stage gas electron multiplier (Triple-GEM) to detect the ionization from  $^{55}\text{Fe}$  X-rays and electrons from  $^{106}\text{Ru}$ . The device allows to perform moderate energy spectroscopy measurements (20 % FWHM at 5.9 keV X-rays) using only digital readout and two discriminator thresholds. Being a truly 2D-detector, it allows to observe individual clusters of minimum ionizing charged particles in  $\text{Ar}/\text{CO}_2$  (70:30) and  $\text{He}/\text{CO}_2$  (70:30) mixtures and to achieve excellent spatial resolution for position reconstruction of primary clusters down to  $\sim 50 \mu\text{m}$ , based on the binary centroid determination method.

*Key words:* High Energy Physics; Gas Electron Multiplier; Medipix2 Chip; CMOS ASIC; Gaseous Pixel Detector; Point Resolution

*PACS:*

---

## 1 Introduction

The development of Micro-Pattern Gas Detectors (MPGD), which has been initiated and still driven by elementary particle and nuclear physics, offers a great potential as a high resolution tracking detector for a variety of applications. Recent advances in photolithography and microprocessing techniques from chip industry triggered the development of more powerful detector concepts, such as Gas Electron Multiplier (GEM) [1] and the MICRO MESH

---

<sup>1</sup> now at Rheinische Friedrich-Wilhelms-University, Department of Physics, Bonn, Germany

GAseous Structure (Micromegas) [2]. The COMPASS fixed-target experiment at CERN has pioneered the use of large area multi-GEM and Micromegas detectors for particle tracking at high intensities, reaching  $5 \text{ kHz/mm}^2$  close to the beam. Both technologies have achieved tracking efficiency close to 100 %, spatial resolution of the order of 70 - 100  $\mu\text{m}$  and time resolution of  $\sim 10 \text{ ns}$  [3], [4]. The excellent performance and radiation hardness of GEM and Micromegas detectors after several years of successful running in COMPASS has demonstrated the large-scale feasibility and robustness of the MPGD concept. GEM detectors have also entered the LHC project; they will be used in the LHCb Muon detector [5] and in the TOTEM telescopes [6].

Recently, Micro-Pattern Gas Detectors were readout by high granularity CMOS pixel chips with integrated amplification and digitization circuits (PixelASICs). This technique opens novel detection possibilities for the application of MPGDs in the future generation of particle and astrophysics experiments. A GEM detector coupled to a CMOS analog chip, comprising pixellated charge collecting electrodes and readout electronics, can reconstruct the tracks of  $^{55}\text{Fe}$  photoelectrons with a length as short as few hundred microns [7]- [10]. Another possible active pixel anode plane for X-Ray Polarimetry is an amorphous silicon thin-film transistor (TFT) array, like those used in flat-panel monitors [11]. The use of pixellated gas detectors to enable true imaging of charged particle tracks has been also proposed for an advanced Compton Telescope [12]-[14] and for the search of Weakly Interacting Massive Particles [15].

The application of Micro-Pattern Gas Detectors for high precision tracking at the future International Linear Collider (ILC) is an active field of R&D in detector technology. A Time Projection Chamber (TPC) using MPGDs as a gas amplification device is one of the main options for charged particle tracking [16], [17]. *R&D* is carried out within the ILC TPC collaboration aiming at the construction of a large prototype in the coming years. While the standard approach to readout the signals is a segmented pad plane with front-end electronics attached through connectors from the backside, an attractive possibility is the use of PixelASICs to serve as integrated device hosting the pad, the preamplification and the digitization and sparsification of the signals. This approach could offer an ultimate TPC resolution and a possibility to observe individual electrons formed in the gas and count the number of ionization clusters per unit track length for particle discrimination [18]. Earlier studies using GEM and Micromegas mounted on the Medipix2 chip provided two-dimensional images of minimum ionizing track clusters [19] -[21].

In the following, we present results obtained with a Triple-GEM detector readout with Medipix2 ASIC, and irradiated with  $^{55}\text{Fe}$  X-rays and  $^{106}\text{Ru}$  electrons. An overview of the Triple-GEM / Medipix2 Detector, built at Freiburg University, and of the Medipix2 readout and calibration system is given in Section 2. In Section 3.1, results obtained with the  $^{55}\text{Fe}$  source, including charge spec-

troscopy measurements using the dual threshold capability of the Medipix2 digital readout, are described. In Section 3.2, results obtained with electrons from the  $^{106}\text{Ru}$  source are summarized. They include the measurement of the spatial resolution for primary ionization clusters in  $\text{Ar}/\text{CO}_2$  and  $\text{He}/\text{CO}_2$  gas mixtures. Finally, long-term stability and operational experience with the present setup is discussed.

## 2 The Triple-GEM / Medipix2 Detector

### 2.1 Experimental Setup

The Triple-GEM/Medipix2 detector, built at Freiburg University, consists of three cascaded GEM multiplication stages coupled to a multi-pixel ASIC developed at CERN (“Medipix2”) with individual pixels that amplify, discriminate and count individual hits [22],[23]. The chip is designed and manufactured in a six-metal  $0.25\ \mu\text{m}$  CMOS technology. Fig. 1 shows the schematic layout of the setup and the enlarged photo of the Medipix2 ASIC.

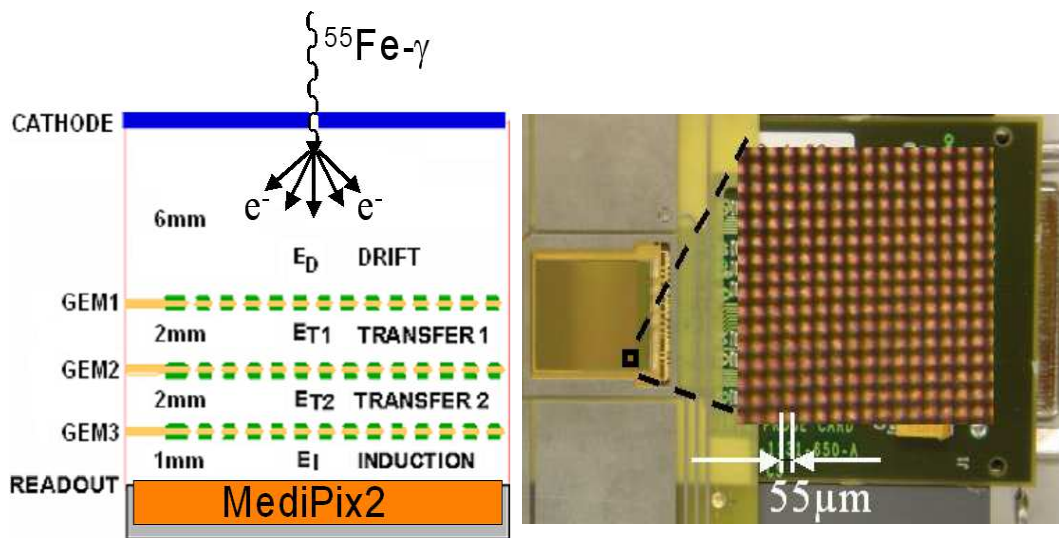


Fig. 1. (Left) A schematic drawing of the GEM/Medipix2 detector.  $E_D$ ,  $E_T$  and  $E_I$  are the drift, transfer and induction field, respectively. (Right) Enlarged photo of Medipix2 pixel cells; a  $25\ \mu\text{m}$  wide conductive bump bond openings, used for electron collection, are seen as a matrix of dots.

The CERN-produced GEMs with double-conical holes, of  $10 \times 10\ \text{cm}^2$  size, have a standard thickness of  $50\ \mu\text{m}$  with holes, arranged in a hexagonal pattern, of  $140\ \mu\text{m}$  pitch and  $70\ \mu\text{m}$  diameter (in Cu). Application of a suitable voltage difference between the metal layers of the GEM produces a strong electric field in the holes ( $\sim 50 - 100\ \text{kV/cm}$ ), where the gas amplification

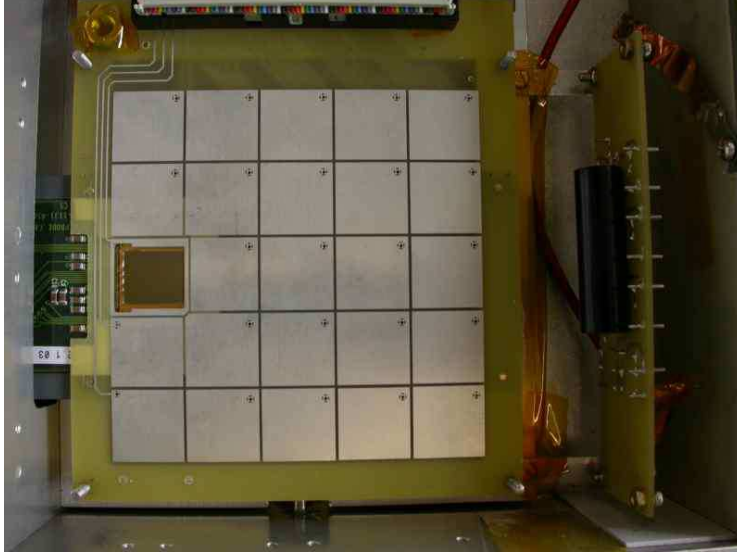


Fig. 2. Photo of the charge collection plane (anode) consisting of 25 pads, with one pad area replaced by the Medipix2 chip.

occurs. In multiple GEM structures there are 3 different electron drift regions: in our setup, the drift gap (where the primary electrons are created) of 6 mm has been chosen, while the transfer region (between successive GEMs) and the induction gap (between the last GEM and readout plane) are 2 and 1 mm, respectively. The  $10 \times 10 \text{ cm}^2$  charge collection plane consists of 25 pads, each connected to a discrete preamplifier-discriminator chain, developed for the L3 Forward Muon Detector [24]. Into one of the pads (approximately  $1.8 \times 1.8 \text{ cm}^2$ ), a “naked” Medipix2 chip (without a silicon detector bonded) is inserted (see Fig. 2). The Medipix2 sensitive area is arranged as a square matrix of  $256 \times 256$  pixels of  $55 \times 55 \mu\text{m}^2$  size, resulting in a detection area of  $1.98 \text{ cm}^2$  which represents 87 % of the entire surface area. The periphery, placed at one side of the chip, includes the  $I/O$  control logic, 13 8-bit DACs and 127 IO wire-bonding pads, arranged in a single row [22],[23]. The output of the Medipix2 preamplifier feeds two identical discriminator branches (low and high thresholds), which can be set independently. Each pixel contains an 8bit configuration register. Six bits are used for the threshold equalization (three-bits for each discriminator), one for masking noisy pixels and one to enable the test input pulse through the 8 fF-on-pixel capacitor. Using the serial or parallel readout interface, the readout of the whole pixel matrix containing measured data takes 9 ms or  $266 \mu\text{s}$ , respectively, for a 100 MHz clock.

Approximately 75 % of each pixel is covered with an insulating passivation layer. Thus electrical field lines end on the conductive bump-bonding pads (octagonally shaped,  $25 \mu\text{m}$  wide) exposed to the gas (see Fig. 1 (right)). Only electrons moving in the induction gap contribute to the signal. The time development of the signal is fast as the transit time of electrons in 1 mm induction gap is approximately 20 ns. The signal at the Medipix2 input is proportional to the charge, which is collected on the bump-bonding pad in

each pixel. This makes use of Medipix2 ASIC as a charge collecting anode and the pixel segmented readout of a GEM detector, allowing a true 2D image reconstruction.

## 2.2 Medipix2 data readout and calibration

The Medipix2 chip was controlled and read out by the MUROS2 electronics [25] and the software “Medisoft 4.0” developed by University of Naples [26]. Using a clock of 50 MHz in our setup, the pixel matrix was readout in about 20 *ms* in serial mode. To minimize the impact of threshold non-uniformity across the channels, the optimization of the Medipix2 settings in Freiburg involved the equalization of low (*THL*) and high (*THH*) thresholds by applying an external test pulse to the on-pixel 8 fF injection capacitance [23]. Using a pixel test input a threshold scan for a fixed pulse charge is performed to measure *S*-shaped curves for each channel: from no pixel counts (0 % efficiency) to 100 % hits for low threshold (*THL*) and, for larger input charges, from 100 % efficiency to no counts for the high threshold (*THH*). The threshold dispersion between pixels is tuned based on the 50 %-efficiency point of the *S*-curve using the 3-bit-DAC available in each discrimination branch. The difference in charge corresponding to 97.7 % and 2.3 % of the *S*-function, divided by factor of four, is used as a measure of the equivalent noise charge (ENC) of the pixel analog section, assuming a Gaussian distribution.

A dedicated study was performed in order to obtain an absolute calibration of the Medipix2 chip - to match low and high threshold *DAC* settings (*THL* and *THH*) to the corresponding effective charges in electrons ( $q_{THL}$  and  $q_{THH}$ ). In conventional Medipix setup the chip is connected to a Si semiconductor detector allowing direct energy calibration with radioactive sources. For our applications - we used a “naked” Medipix2 chip without *X*-ray converter - calibration can only be performed using the electrical input pulse. In a first step, the resulting charge  $Q_{input}^{test}$  (in  $e^-$ ) appearing at the amplifier input can be estimated as a function of applied voltage step  $\Delta V$ :

$$Q_{input}^{test} = \frac{0.825 \cdot 8fF}{1,6 \cdot 10^{-19}} \cdot \Delta V, \quad (1)$$

where 0.825 is the amplification of the analog buffers used to transmit the external test pulse to each pixel.

Since it is known, that the behavior of the input buffers of the charge injection circuit is non-linear for large input voltages ( $> 100$  mV) we correct the obtained threshold charges  $Q_{input}^{test}$  in Eq. 1 for the measured difference in response between various gamma sources and injected test pulses for another Medipix2

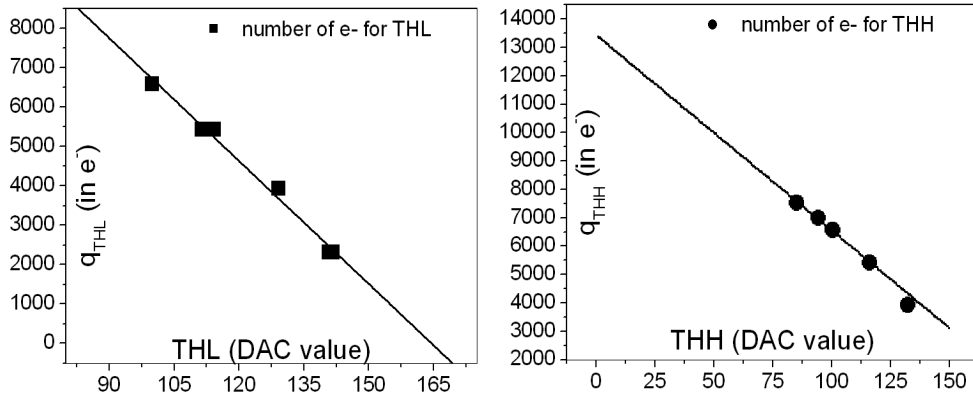


Fig. 3. Medipix2 calibration curves matching  $DAC$  settings for the low and high threshold values ( $THL$  and  $THH$ ) to the effective charges in electrons ( $q_{THL}$  and  $q_{THH}$ ).

ASIC, bonded to a  $300\mu m$  wafer of silicon [27]. From this procedure, we obtain calibration curves for the  $THL$  and  $THH$   $DAC$  values shown in Fig. 3. Applying the threshold equalization and using this calibration, we estimate the minimum operational low threshold  $q_{THL}$  in our setup to be approximately 990 electrons with an uncertainty of 140 electrons, resulting from the linear extrapolation of the calibration curve in Fig. 3.

### 3 Measurements and Results

The performance of the Triple-GEM / Medipix2 detector was studied with  $^{55}\text{Fe}$  X-Rays and  $^{106}\text{Ru}$  electrons. The  $^{55}\text{Fe}$  5.9 keV X-ray produces an ionization cluster in the detector volume, corresponding to approximately 220 primary electrons in  $\text{Ar}/\text{CO}_2$ . The  $^{106}\text{Ru}$  source emits electrons with a maximum kinetic energy of 3.54 MeV from the decay of  $Rh^{106}$ , which leaves the ionization track with approximately 60 (20) primary electrons per cm in  $\text{Ar}/\text{CO}_2$  ( $\text{He}/\text{CO}_2$ ) mixtures (see Table 1).

#### 3.1 $^{55}\text{Fe}$ X-rays in $\text{Ar}/\text{CO}_2$ (70:30)

The GEM/Medipix2 detector system, was exposed to  $^{55}\text{Fe}$  X-rays, entering the detector through the cathode drift electrode (see Fig. 1 (left)). Most of the X-rays are converted in the drift gap in  $\text{Ar}/\text{CO}_2$  (70:30) mixture emitting a photo-electron, which produces a short ionization track in the gas. The cloud of primary electrons from the track drift through the multi-GEM structure, where they are multiplied and then collected on the input pads of Medipix2 chip (see Fig. 1 (right)). Standard high voltage settings for  $\text{Ar}/\text{CO}_2$  (70:30) operation were: drift field  $E_D = 1.1$  kV/cm, transfer field  $E_T = 3.2$  kV/cm,

induction field  $E_I = 4.2$  kV/cm, grounded anode readout plane and  $\Delta V_{GEM1} = \Delta V_{GEM2} = \Delta V_{GEM3} = 404$  V, corresponding to a gas gain of approximately  $6 \times 10^4$  (see Fig. 7).

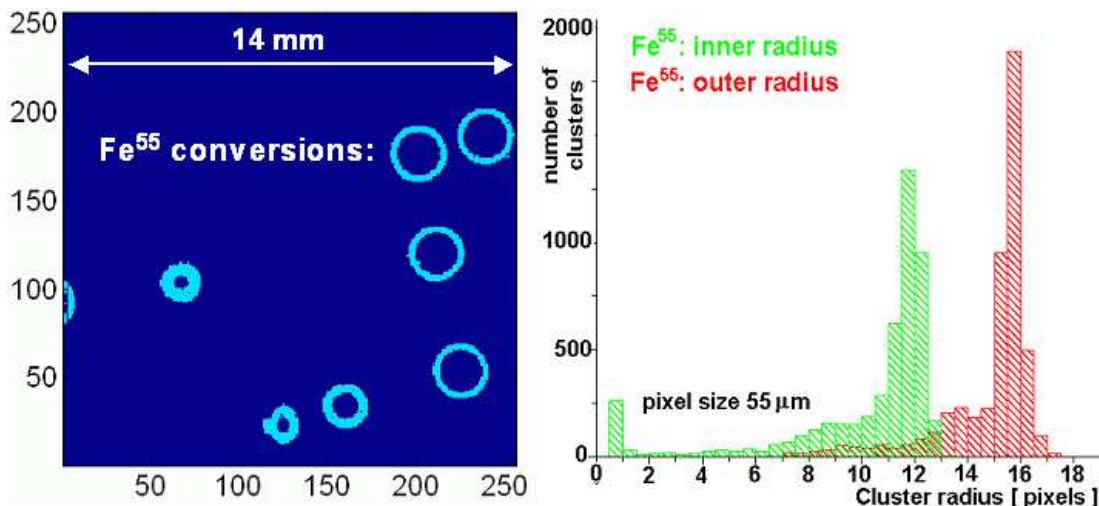


Fig. 4. (Left) Medipix2 images of  $^{55}\text{Fe}$  conversions. (Right) Distributions of inner and outer cluster radius of  $^{55}\text{Fe}$  “donuts” for chip operated in the charge window mode (see text).

The Medipix2 chip does not provide pulse height information, but it can be operated in the charge window mode [22]. In this operation mode, the detected electron charge in each pixel is amplified and then compared with Medipix2 low ( $q_{THL}$ ) and high ( $q_{THH}$ ) thresholds that form effectively a charge window  $\Delta W = q_{THH} - q_{THL}$ . If the detected charge falls inside this window ( $\Delta W$ ) a 13-bit digital counter is incremented. With a digital readout in charge window mode, the  $^{55}\text{Fe}$  conversions are seen as “donuts” of different sizes, according to the deposited energy. Fig. 4 (left) shows images of  $^{55}\text{Fe}$  quanta conversions, acquired without external trigger during approximately 1 s of Medipix2 acquisition time. To record this image the effective low and high thresholds were set to:  $q_{THL} \approx 990 e^-$  (DAC  $THL$  value = 155) and  $q_{THH} \approx 12000 e^-$  (DAC  $THH$  value = 20), respectively (see Fig.3). A sample of  $^{55}\text{Fe}$  images was collected with these settings. Fig. 4 (right) reveals clear peaks in the distributions of inner ( $r_{THH}$ ) and outer ( $r_{THL}$ ) radius of nearly circular “donuts”, which correspond to photoelectric conversions of 5.9 keV  $X$ -rays, with tails mostly coming from  $Ar$ -escape electrons and background events.

The operation of the Medipix2 ASIC in the charge window mode also allows us to perform an estimation of the total cluster charge in “donuts”. The procedure is illustrated in Fig. 5. Assuming a conical shape of the charge cloud (the assumption of a more realistic Gaussian profile would not alter the results significantly) and using the inner ( $r_{THH}$ ) and outer ( $r_{THL}$ ) radius of the “donut” for the corresponding settings of low ( $q_{THL}$ ) and high ( $q_{THH}$ ) thresholds, the

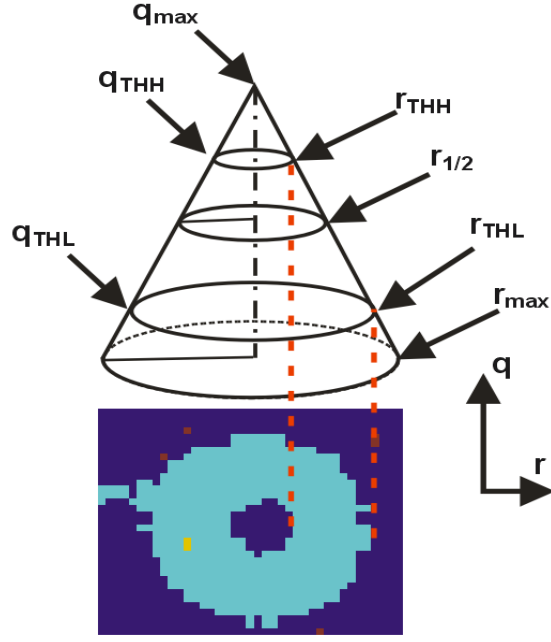


Fig. 5. Schematics used for the calculation of the total cluster charge  $Q$  from the inner ( $r_{THH}$ ) and outer ( $r_{THL}$ ) radii of the “donut” for the low ( $q_{THL}$ ) and high ( $q_{THH}$ ) Medipix2 thresholds and assuming a conical shape of the charge cloud collected on the Medipix2 bump-bonding pads.

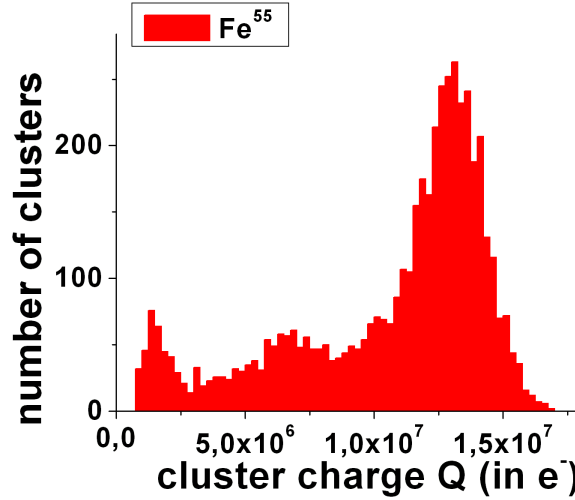


Fig. 6. Distribution of the cluster charge  $Q$  in “donuts” for the 5.9 keV  $X$ -rays, reconstructed using the method described in Fig. 5.

total cluster charge  $Q$  can be estimated as:

$$Q = \frac{1}{3} \pi \cdot r_{max}^2 \cdot q_{max}, \quad (2)$$

$$q_{max} = \frac{r_{THL} \cdot q_{THH} - r_{THH} \cdot q_{THL}}{r_{THL} - r_{THH}}, \quad (3)$$

$$r_{max} = \frac{r_{THL} \cdot q_{THH} - r_{THH} \cdot q_{THL}}{q_{THH} - q_{THL}}, \quad (4)$$



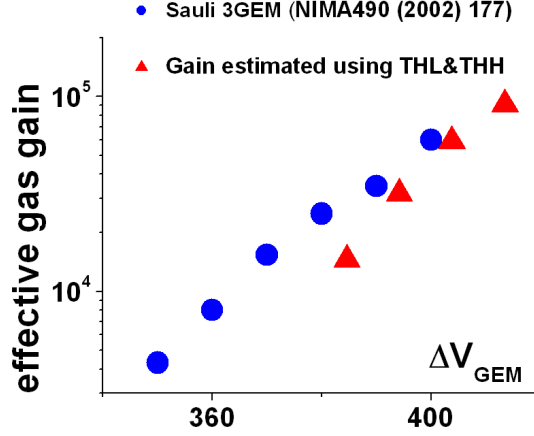


Fig. 7. Effective gas gain in  $Ar/CO_2$  (70:30) calculated from the cluster charge  $Q$  in “donuts” (dots) and compared to the gas gain values, derived from the measurement of the current for a known radiation flux (triangles) in [28].

where  $r$  is a dimensionless parameter, measured in number of pixels,  $q$  is a charge (in electrons).

Fig. 6 represents the distribution of the total cluster charge  $Q$  deposited by  $^{55}Fe$  5.9 keV  $X$ -rays. The  $Ar$ -escape peak and photo-peak are clearly visible and separated. The energy resolution of the “charge spectroscopy” method is approximately 20% full-width at half-maximum (FWHM) for an  $X$ -ray energy of 5.9 keV. By varying voltage across GEMs, the effective gas gain was determined from the central value of the photo-peak in the cluster charge distribution and the assumption that  $^{55}Fe$  quanta generate 220 primary electrons in  $Ar/CO_2$ . The results shown in Fig. 7 are very similar to the absolute gain calibration, derived from the measurement of the current for a known radiation flux in [28].

### 3.2 $^{106}Ru$ electron tracks in $Ar/CO_2$ (70:30) and $He/CO_2$ (70:30)

With the GEM/Medipix2 detector we collected a sample of tracks from a radioactive  $^{106}Ru$   $\beta^-$ -source for two different gas mixtures,  $Ar/CO_2$  (70:30) and  $He/CO_2$  (70:30). The gas gains were  $6 \times 10^4$  ( $\Delta V_{GEM} = 404$  V) and  $2 \times 10^5$  ( $\Delta V_{GEM} = 428$  V) for the  $Ar$  and  $He$ -based mixtures, respectively. To record track images a four-fold coincidence of conventional readout pads in a row, with a pixel chip positioned between them, was used to trigger the Medipix2 readout (see Fig. 8). For these measurements, the chip was operated in a single discrimination mode (only low THL threshold was used).

A recorded two-dimensional image of an electron track from  $^{106}Ru$  in  $Ar/CO_2$

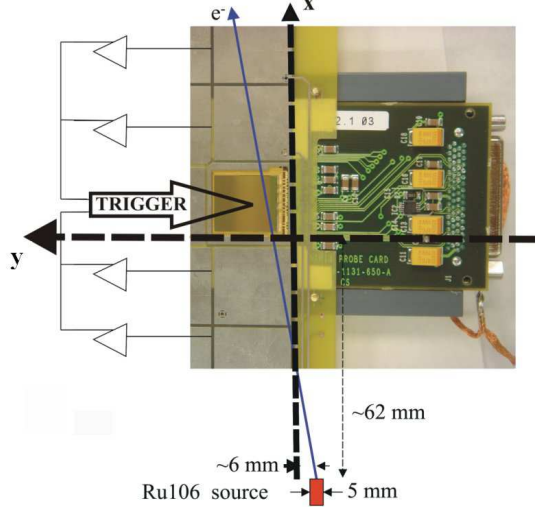


Fig. 8. Schematics of signal coincidence from four conventional readout pads used to trigger Medipix2 readout. The relative position of  $^{106}\text{Ru}$  source with respect to pixel ASIC in  $(x,y)$  plane is also indicated.

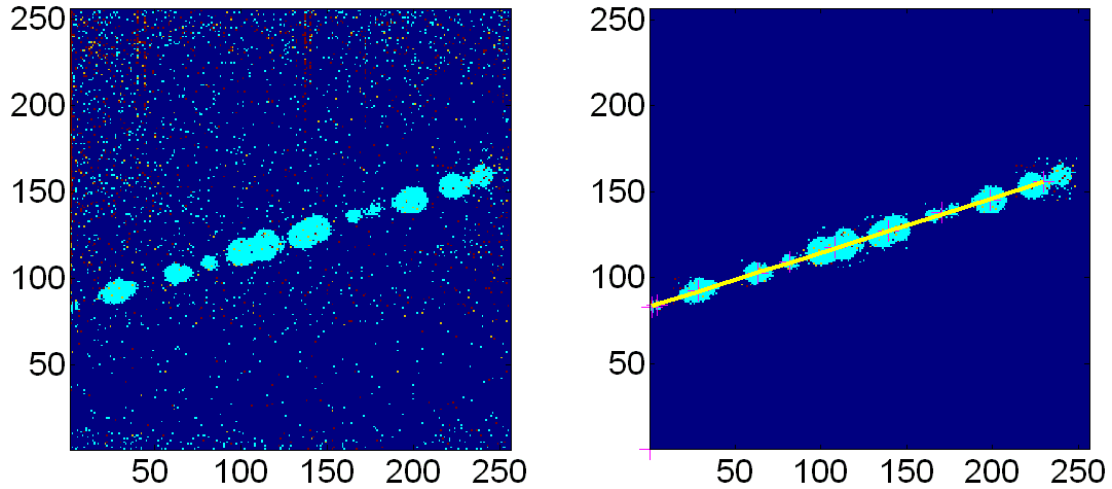


Fig. 9. (Left) “Raw” Medipix2 image of the electron track from  $^{106}\text{Ru}$  source in  $\text{Ar}/\text{CO}_2$  (70:30). (Right) Straight line fit to the centers of clusters after the noise suppression procedure (isolated noise hits, which are collected due to the relatively long recording time (up to 1 s), are suppressed).

(70:30) is illustrated in Fig.9 (left) along with a straight line fit to the reconstructed centers of clusters in Fig.9 (right). The recorded electron track consists of clearly visible extended charge clusters. The observed cluster size varies considerably due to the fluctuating number of primary ionization electrons per cluster and variations in the gas multiplication. The average spatial extent of charge clouds on the Medipix2 surface depends on the sizes of the transfer and induction gaps and the electric fields strength  $E_T$ ,  $E_I$  and  $\Delta V_{GEM}$ . The distribution of the *RMS* spread of the cluster centers from a straight line track is mainly determined by the electron diffusion in the drift region. Fig. 10 (left) shows an image of an energetic  $\delta$ -electron liberated in  $\text{He}/\text{CO}_2$ . Based

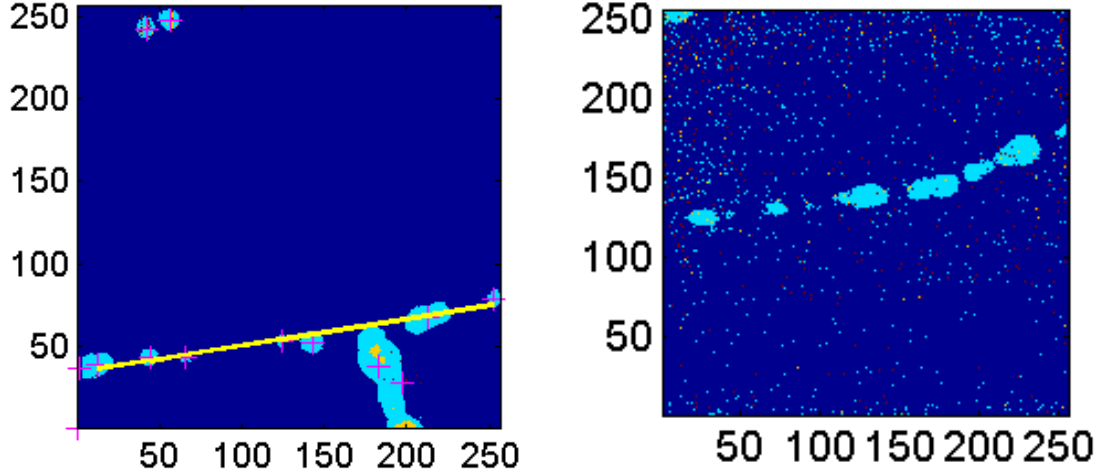


Fig. 10. Medipix2 image of  $\delta$ -electron liberated in  $He/CO_2$  (70:30) with energy  $E_\delta > 10$  keV (left).  $^{106}Ru$  electron track that suffered multiple Coulomb scattering in  $Ar/CO_2$  (70:30) (right).

on the visible  $\delta$ -electron range  $R > 3.5$  mm, its energy  $E_\delta$  can be estimated to be more than 10 keV.

Gas mixture	$n_p^e$	$n_p^\pi$	$n_T^e$	$n_T^\pi$	$X_{rad}$ (m)	$\rho$ ( $g/cm^3$ )
$Ar/CO_2$ (70 : 30)	28.9	30.3	62.8	76.4	125	$1.8 \cdot 10^{-3}$
$He/CO_2$ (70 : 30)	13.0	13.6	20.7	25.4	565	$0.7 \cdot 10^{-3}$

Table 1

Number of primary ionization clusters  $n_p^e$  and total electron-ion pairs  $n_T^e$  produced in 1 cm of  $Ar/CO_2$  (70:30) and  $He/CO_2$  (70:30) for 2 MeV electrons, as generated by HEED simulation program [29]. The corresponding numbers ( $n_p^\pi, n_T^\pi$ ) for minimum ionizing particles (e.g. 0.6 GeV pions) are presented for comparison. Radiation lengths  $X_{rad}$  and gas mixture densities  $\rho$  ( $g/cm^3$ ) for both mixtures are also given.

With an effective threshold of  $q_{THL} \approx 990e^-$ , on average  $N_{cl}^{obs} \approx 8$  clusters per track were reconstructed in both mixtures. This number has to be compared with the expected number of primary electron clusters  $n_p^e$  released by a  $\approx 2$  MeV  $\beta^-$  track in a specific gas mixture (see Table 1). The determination of the efficiency for reconstructing a single or multi-electron cluster, which requires a careful comparison with simulation, is under study. Here, we only give approximate estimate for the detection efficiencies. Based on simulations from the HEED program [29],  $n_p^e \approx 40.5$  (18.2) primary ionization clusters are expected along a track of 1.4 cm length in  $Ar/CO_2$  ( $He/CO_2$ ). Thus, the average efficiency to reconstruct a primary ionization cluster is approximately 20 % (45 %). Due to the fluctuations in the multiplication process in the GEMs we do not attempt to estimate the single electron efficiency at this stage. However, it is obvious that the single electron efficiency is non-zero. In particular, for  $He/CO_2$  mixture only 3.2 multi-electron clusters are expected on average along a 1.4 cm track (see Table 2), to be compared with  $N_{cl}^{obs} \approx 8$  recorded clusters.

$k(e^-)$	1	2	3	4	$\geq 5$
$P(k)$ (%) for $Ar/CO_2$	80.4	8.6	2.6	1.4	7.0
$P(k)$ (%) for $He/CO_2$	81.6	11.0	2.9	1.2	3.0

Table 2

Cluster-size distribution probability  $P(k)$  (in %) of producing exactly  $k$  ionization electrons for 2 MeV electrons in  $Ar/CO_2$  (70:30) and  $He/CO_2$  (70:30) mixtures, as generated by HEED simulation program [29].

In the following data analysis we focus on the achievable single point resolution with the digital readout of the GEM/Medipix2 detector. The following criteria were applied to select events, which were included in this analysis:

- A cluster is defined as a set of more than 4 adjacent hit pixels;
- The distance between two neighbored track clusters has to be smaller than 50 pixels (both in  $x$  and  $y$  directions);
- More than 5 clusters per track are required;
- Events with multiple tracks are rejected.

A total of several hundred tracks were selected by this procedure for  $Ar/CO_2$  and  $He/CO_2$  gases. First, we perform a two-dimensional straight line fit to the cluster centers and calculate the distance between each cluster center and the position of the point of closest approach along the fitted track. The corresponding distributions, when all  $N_{cl}$  cluster centers are included in the track fit, are shown in Fig. 11. The standard deviations,  $\sigma_N$ , of a Gaussian fit to the residual distributions gives  $64 \pm 2 \mu m$  for  $Ar/CO_2$  (70:30) and  $58 \pm 2 \mu m$  for  $He/CO_2$  (70:30) gas mixtures (see Table 3). In a second step, we repeat this procedure but omitting the cluster under consideration from the track fit. The corresponding distributions, when the track fit is performed to  $N_{cl} - 1$  clusters, is shown in Fig. 12. The standard deviations,  $\sigma_{N-1}$ , are  $84 \pm 3 \mu m$  and  $73 \pm 3 \mu m$ , respectively. An unbiased estimate for the single point resolution  $\sigma_{mean}$  is obtained as the geometric mean of two methods [30]:

$$\sigma_{mean} = \sigma_N \cdot \sigma_{N-1}, \quad (5)$$

The corresponding resolutions are summarized in Table 3.

In addition to inelastic collisions with atomic electrons, a few MeV  $^{106}Ru$  electrons also suffer Coulomb scattering from nuclei, which increases the standard deviations of residuals ( $\sigma_N$  and  $\sigma_{N-1}$ ) from the straight line fit. This effect can be clearly seen from the image of a “curved” electron track in Fig. 10 (right). We also calculated the “3-point” resolution, which is much less sensitive to multiple scattering effects. For any three consecutive clusters ( $i - 1, i, i + 1$ ) the “3-point” method calculates the difference between the measured cluster  $i$ , and the position predicted from a straight line between cluster centers  $i - 1$

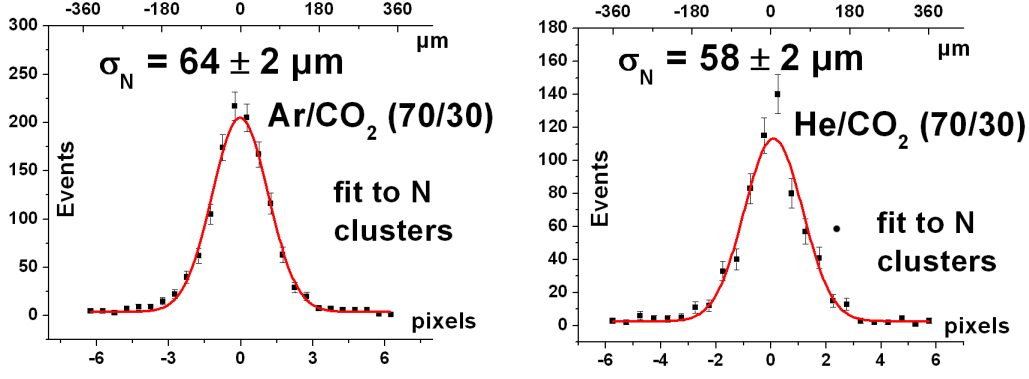


Fig. 11. Single point resolution ( $\sigma_N$ ) for  $Ar/CO_2$  (70:30) (left) and  $He/CO_2$  (70:30) (right) when all  $N_{cl}$  cluster centers are included in the track fit. The residual distributions are well described by a single Gaussian.

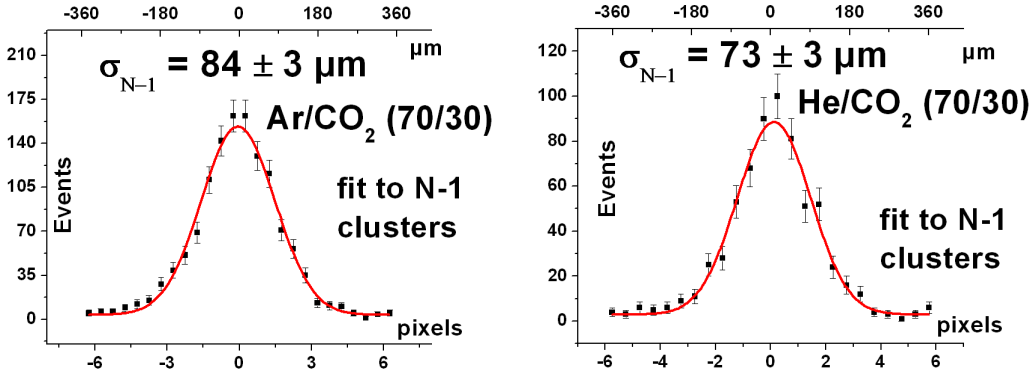


Fig. 12. Single point resolution ( $\sigma_{N-1}$ ) for  $Ar/CO_2$  (70:30) (left) and  $He/CO_2$  (70:30) (right) when the track fit is performed to  $N_{cl} - 1$  clusters, excluding cluster under study.

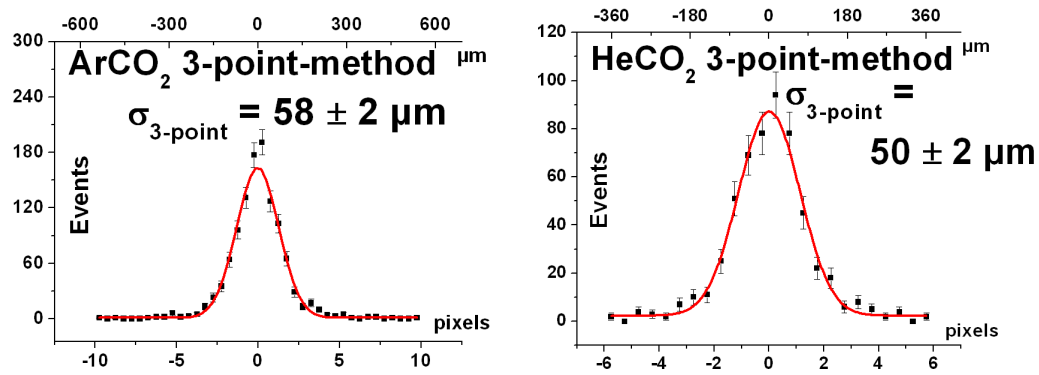


Fig. 13. The 3-point resolution ( $\sigma_{3-point}$ ) for  $Ar/CO_2$  (70:30) (left) and  $He/CO_2$  (70:30) (right).

and  $i + 1$ . The “3-point” resolution ( $\sigma_{3-point}$ ) is obtained by multiplying the  $RMS$  of residuals by a factor of  $\sqrt{2/3}$ , which yields an unbiased estimate of the single point resolution for the equally spaced points. Here, the fit results are  $71 \mu m$  ( $61 \mu m$ ) and the corresponding “3-point” resolutions ( $\sigma_{3-point}$ )

Gas mixture	$\sigma_N(\mu m)$	$\sigma_{N-1}(\mu m)$	$\sigma_{mean}(\mu m)$	$\sigma_{mean}^{corr}(\mu m)$	$\sigma_{3-point}(\mu m)$
$Ar/CO_2(70 : 30)$	$64 \pm 2$	$84 \pm 3$	$73 \pm 3$	$\sim 54$	$58 \pm 2$
$He/CO_2(70 : 30)$	$58 \pm 2$	$73 \pm 3$	$65 \pm 3$	$\sim 61$	$50 \pm 2$

Table 3

Summary of resolution studies in  $Ar/CO_2$  (70:30) and  $He/CO_2$  (70:30) mixtures using various evaluation methods:  $\sigma_{mean}$  - unbiased spatial resolution, derived from geometric mean of two standard deviations  $\sigma_N$  and  $\sigma_{N-1}$  (see Eq. 5 for details);  $\sigma_{mean}^{corr}$  - single point resolution, determined from  $\sigma_{mean}$  by correcting for multiple scattering effects,  $\sigma_{3-point}$  - “3-point” resolution values.

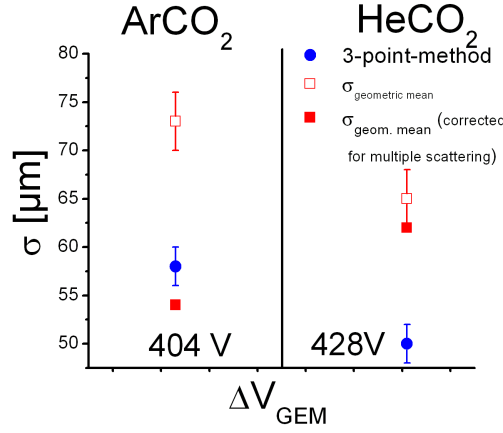


Fig. 14. Summary of transverse single point resolution in  $Ar/CO_2$  (70:30) and  $He/CO_2$  (70:30) mixtures using Medipix2 binary readout and centroid determination method.

are  $58 \mu m$  ( $50 \mu m$ ) for the  $Ar/CO_2$  and  $He/CO_2$  mixtures, respectively (see Fig. 13). The geometric mean method ( $\sigma_{mean}$ ) gives a somewhat larger values compared to the “3-point” values ( $\sigma_{3-point}$ ) for both gases, owing to the non-negligible multiple scattering contribution of  $\approx 2$  MeV electrons to the achievable spatial accuracy.

The effects of Coulomb scattering on the track parameters can be approximated by the appearance of the track curvature  $c = 1/R$  for the otherwise unscattered straight-line tracks. The corresponding multiple scattering ( $\sigma_{mult\ scat}$ ) contribution to the point measuring accuracy ( $\sigma_{mean}$ ) can be evaluated from the variance of the electron trajectory  $y = f(x) \sim x^2/2R$  over the track length of  $L$ :

$$\sigma_{mult\ scat} = \langle y^2 \rangle - \langle y \rangle^2 = \left(\frac{1}{2R}\right)^2 \cdot \left(\frac{L}{2}\right)^4 \cdot \left(\frac{1}{5} - \frac{1}{9}\right) \quad (6)$$

The variance  $[c^2]$  of the total curvature, due to the multiple scattering, depends on the particle velocity  $\beta$  and the momentum  $p$  as well as on the radiation

length  $X_{rad}$  of the gas mixture [31]:

$$[c^2] = (\delta \frac{1}{R})^2 = (\frac{21 \text{ MeV}}{\beta c p})^2 \cdot \frac{1}{X_{rad}} \cdot \frac{C_N}{2L}. \quad (7)$$

The track length  $L$  is measured in the Medipix2 plane ( $L \approx 1.4 \text{ cm}$ ) and the constant  $C_N$  is equal to  $\approx \sqrt{2}$ . By inserting  $(1/R)$  from Eq. 7 to the Eq. 6, we may express the corresponding multiple scattering term as:

$$\sigma_{mult \text{ scat}} = \frac{21 \text{ MeV}}{\beta c p} \sqrt{\frac{\sqrt{2}}{128} \cdot \frac{L^3}{X_{rad}} \cdot (\frac{1}{5} - \frac{1}{9})}. \quad (8)$$

Substituting the numerical values in Eq. 8 and assuming the electron momentum of  $p \approx 2 \text{ MeV}$  one gets  $\sigma_{mult \text{ scat}} \approx 49 \text{ } \mu\text{m}$  ( $23 \text{ } \mu\text{m}$ ) for the *Ar* and *He*-based mixtures, respectively. The corrected values for the achievable single point accuracy, obtained by quadratic subtraction of the multiple scattering contribution:  $\sigma_{mean}^{corr} = \sqrt{\sigma_{mean}^2 - \sigma_{mult \text{ scat}}^2}$ , are between  $50 \text{ } \mu\text{m}$  and  $60 \text{ } \mu\text{m}$ , being consistent with “3-point” resolution results (see Table 3 and Fig. 14) for *Ar/CO<sub>2</sub>*. For *He/CO<sub>2</sub>* small discrepancy still remains.

Despite the large width of charge clouds ( $\geq 10$  pixels) in the GEM/Medipix2 readout plane (see Fig. 9), this result demonstrates the possibility to achieve spatial resolution of the order of the pixel width, based on the centroid determination method and digital Medipix2 readout.

## 4 Long-Term Stability

A very attractive feature of the GEM is that it allows to completely decouple charge amplifying region (GEM) from the collecting electrodes - printed circuit board, which operate at a unity gain. To date, no single Medipix2 chip, exposed to an induction field of  $E_D \sim 4 \text{ kV/cm}$ , has been destroyed due to the electrostatic or GEM discharges in our triple GEM setup after several months of operation during the time-span of more than one year. No damage to a pixel VLSI analog chip used as a direct anode of single GEM has been also observed in [8]. This proves that the reliable operation can be established for GEM gas amplification coupled to *Si*-pixel readout and that the propagation of destructive discharges to the sensitive CMOS electronics is strongly suppressed even at large gas gains of  $10^4 - 10^5$ .

## 5 Summary

The Medipix2 chip, being originally developed for a single photon counting, has been successfully adapted as a highly integrated pixel-segmented anode readout of a gas-filled detector, using a triple-GEM as a charge-multiplier. The CMOS readout concept offers the possibility of pixel sizes small enough to observe individual primary electron clusters of minimum ionizing particle tracks and to provide real two-dimensional images of physics events. The approach holds a great potential for high-precision particle tracking at the next generation of high energy physics colliders and for astrophysical applications.

To evaluate the GEM/Medipix2 performance, we have carried out studies with  $^{55}\text{Fe}$  and  $^{106}\text{Ru}$  sources. The Triple-GEM / Medipix2 detector allows to perform energy-sensitive charge spectroscopy measurements (20 % FWHM at 5.9 keV  $X$ -rays) using only digital readout and two discriminator thresholds. In the tracking applications, the detector has been shown to achieve an excellent spatial resolution of  $\sim 50\ \mu\text{m}$ , based on the binary centroid determination of the charge clouds, and allows to reconstruct tracks as short as  $\sim 1.5\ \text{cm}$  length.

For the ILC applications the use of CMOS pixel ASIC in the TPC readout plane will allow to observe individual electron clusters in 3D and fully exploit unprecedented 3D-granularity for the gaseous tracking and to minimize the material in the endplate, since front-end electronics is naturally integrated into the readout pad plane. A modification of the Medipix2 chip (“TimePix”) to measure also the drift time information of primary electrons is under development [32],[33]. This will enable to measure not only the 2D projection, but also to reconstruct the true 3D-space points of charged particles crossing a large TPC volume. The possibility to use time-over-threshold information for time-walk correction and charge estimation are also foreseen in the chip design.

## Acknowledgments.

We thank the Medipix Collaboration for providing us with several Medipix2 chips, and for the readout software and hardware. We would like to thank to Michael Campbell, Erik Heijne, Xavier Llopart and Fabio Sauli for stimulating discussions and a lot of valuable advices.



## References

- [1] F. Sauli, Nucl. Instr. Meth., A386(1997), 531.
- [2] Y. Giomataris, Nucl. Instr. Meth., A376(1996), 29.
- [3] B. Ketzer et al., Nucl. Instr. Meth., A535(2004), 314.
- [4] C. Bernet et al., Nucl. Instr. Meth., A536(2005), 61.
- [5] M. Alfonsi et al., IEEE Trans. Nucl.Sci. 51(5)(2004), 2135.
- [6] M. Bozzo et al., 2004 IEEE NSS/MIC Conference Record.
- [7] E. Costa et al., Nature, Vol. 411(2001), 662.
- [8] R. Bellazzini et al., Nucl. Instr. Meth., A535(2004), 477.
- [9] R. Bellazzini et al., Nucl. Instr. Meth., A560(2006), 425.
- [10] R. Bellazzini et al., arXiv: physics/0604114, submitted to Nucl. Instr. Meth., A
- [11] J.K. Black et al., Nucl. Instr. Meth., A513(2003), 639.
- [12] P.F. Bloser et al., arXiv: astro-ph/0308331.
- [13] P.F. Bloser et al., New Astronomy Reviews, 48(2004), 299.
- [14] H. Kubo et al., 2004 IEEE NSS/MIC Conference Record.
- [15] H. Sekiya et al., arXiv: astro-ph/0601568.
- [16] T. Behnke et al., TESLA TDR volume IV: A Detector for TESLA, DESY 2001-011, ECFA 2001-209.
- [17] LDC working group, Detector Outline Document for the Large Detector Concept (LDC), see <http://www.ilcldc.org>.
- [18] M. Hauschild, “2D and 3D Cluster Counting with GEMs and small Pads: the digital TPC”, Proceedings of the International Workshop on Linear  $e^+e^-$  Colliders, Jeju, Korea (2002).
- [19] P. Colas et al., Nucl. Instr. Meth., A535(2004), 506.
- [20] M. Campbell et al., Nucl. Instr. Meth., A540(2005), 295.
- [21] M. Chefdeville et al., Nucl. Instr. Meth., A556(2006), 490.
- [22] X. Llopart et al., IEEE Trans. Nucl.Sci. 49(5)(2002), 2279.
- [23] X. Llopart, M. Campbell, Nucl. Instr. Meth., A509(2003), 157.
- [24] The L3 collaboration, Nucl. Instr. Meth., A383(1996), 342.
- [25] D. Bello et al., Nucl. Instr. Meth., A509(2003), 164.

- [26] M. Conti et al., IEEE Trans. Nucl.Sci. 50(4)(2003), 869.
- [27] A. Zwerger, Diploma Thesis, University of Freiburg, (2003), (in german).
- [28] C. Altunbas et al., Nucl. Instr. Meth., A490(2002), 177.
- [29] M. Hauschild, <http://hausch.home.cern.ch/hausch/MediPix.html>
- [30] R.K Carnegie et al., Nucl. Instr. Meth., A538(2005), 372.
- [31] W. Blum, L. Ronaldi, Particle Detection with Drift Chambers, Springer-Verlag, (1993).
- [32] H. van der Graaf et al., “The TimePix R & D Collaboration”, Timepix Proposal, November (2004).
- [33] EUDET: An integrated infrastructure initiative funded under the 6<sup>th</sup> EU framework, see <http://www.eudet.org>